Chapter

Microemulsions as Nanoreactors to Obtain Bimetallic Nanoparticles

Concha Tojo, David Buceta and M. Arturo López-Quintela

Abstract

Microemulsions are frequently used as nanoreactors for the synthesis of bimetallic nanoparticles. The ability to manipulate the metal distribution in bimetallic nanoparticles is essential for optimizing applications, and it requires a deeper understanding of how compartmentalization of reaction medium affects nanoparticle synthesis. A simulation model was developed to predict the atomic structure of bimetallic nanoparticles prepared via microemulsion in terms of metals employed and microemulsion composition. The model was successfully proved by comparing theoretical and experimental Au/Pt STEM profiles. On this basis, the model becomes a strong tool to further enhance our knowledge of the complex mechanisms governing reactions in microemulsions and its impact on final nanostructures. The purpose of this study is to perform a comprehensive kinetic analysis of coreduction of different couple of metals in the light of the interplay between three kinetic parameters: intermicellar exchange rate, chemical reduction rates of the two metals, and reactants concentration. The particular combination of these factors determines the reaction rate of each metal, which in turn determines the final metal arrangement.

Keywords: bimetallic nanoparticles, microemulsions, reduction rate, intermicellar exchange rate, nanocatalysts

1. Introduction

From the pioneering work of Boutonnet et al. [1], the synthesis of nanoparticles in microemulsions has been widely investigated with a variety of technical applications in catalysis [2–4], photonics [5], and energy conversion and storage devices [6–8]. The microemulsion route allows to control the size and composition of nanoparticles. A microemulsion consists of nanometer-sized water droplets dispersed in the oil phase and stabilized by a surfactant film. Reactants can be dissolved in the nano-sized water droplets or reverse micelles and can be exchanged between them by direct material transfer during an interdroplet collision [9]. The intermicellar exchange allows the reactants to be carried by the same droplet, so the chemical reaction can proceed inside the nanoreactor. Due to the space limitation inside the micelle, nucleation and growth of the particle are restricted, so it can result in the formation of size-controlled particles. In spite of the complexity of the reaction medium, microemulsion route has several advantages when compared to traditional methods. The first one is that nanoparticle size is directly controlled by the water/surfactant ratio, so narrow size distributions can be obtained. Another advantage is that surfactants around the nanoparticles can be removed with ease

and nanoparticles can be prepared at room temperature. In addition, the confinement of reactants inside micelles induces important changes in reactant concentrations, which strongly affect the reaction rates. Finally, in relation to catalysis, nanoparticles obtained by the microemulsion route present an improved catalytic behavior than particles with the same composition which are synthesized by traditional procedures [10, 11].

A variety of nanomaterials, ranging from metals [12–14], bimetallic structures [15–17], other inorganic nanoparticles [18–20], and organic compounds [21, 22], has been prepared by this approach. In the field of catalysis, microemulsion approach was successfully used to prepare different nanostructured catalytic materials [2, 10, 17, 23–25].

Nevertheless, microemulsion route present a challenge due to the difficulty in managing the material intermicellar exchange. As mentioned above, reactants are distributed in separate nanoreactors, so the whole process (chemical reaction, nucleation, and subsequent growth to build up final particles) is conditioned by the material exchange between them. This exchange is mainly dictated by the surfactant, which is located on the interface between water and oil phases. The hydrophilic portion of the surfactant is anchored into water and the lipophilic one into oil, forming a film which surrounds the micelle surface. It is believed that, when a micelle-micelle collision is violent enough, the surfactant film breaks up, allowing the material exchange. As a consequence, the rate of intermicellar exchange controls the reactants encounter and therefore plays a key role in chemical kinetics in microemulsions. The ease with which intermicellar channels are established as well as their size and stability are determined by the microemulsion composition, which in turn has been shown to affect final nanoparticle properties [26–28].

In the paper at hand, we are focused on the study of Pt/M (M = Au, Rh) nanoparticles synthesized in microemulsions. Platinum-based nanoparticles (NPs) exhibit remarkable electrocatalytic activity in many important chemical and electrochemical reactions including oxygen reduction reaction (ORR) and direct methanol oxidation [29]. Apart from the inherent chemical and physical properties of the constitutive metals, the catalytic activity, which is one of the more relevant applications of bimetallic nanoparticles, relies notably on the metal distribution, that is, on the intraparticle nanoarrangement [30]. Bimetallic nanoparticles can show four main mixing patterns: (a) core-shell structures, in which one metal forms the core and the second metal covers the first one forming the surrounding shell; (b) mixed structures, which are often called alloys; (c) multilayer structures [31]; and (d) sub-cluster segregated structures, characterized by a small number of heteroatomic bonds [12]. So, the control of bimetallic intrastructure, mainly within the first atomic layers from the surface [25, 32], is key for performance enhancement of bimetallic catalysts. Furthermore, the optimal metal distribution depends on the particular chemical reaction. Au-core/Pt-shell nanocatalyst exhibits an improved activity to catalyze formic acid electro-oxidation [33] or oxygen reduction reaction [34, 35]. On the contrary, an alloyed Pt-Au is better for electro-oxidation of methanol [36]. Therefore, an in-depth study aimed at tailoring well-defined structures will be of great interest.

Although the simultaneous reduction of the two metals by the microemulsion route is one of the most common procedures to control the size and composition of bimetallic nanoparticles [24, 37], the prediction of the resulting metal arrangement is complicated, as far as the current state-of-the-art is concerned. As a matter of fact, many studies designed to produce new nanoarrangements via microemulsions come from trial-and-error experiments, mainly due to the high number of involved synthetic variables and to their interaction with the inherent complexity of the reaction media. A robust tool for elucidating the interplay between the different

factors concerning final bimetallic nanoarrangements is computer simulation. With the aim of understanding the different factors affecting final nanostructures, we perform a comprehensive kinetic analysis of coreduction of different couple of metals in the light of the interplay between three kinetic parameters: intermicellar exchange rate, chemical reduction rates of the two metals, and reactants concentration. The particular combination of these factors determines the reaction rate of each metal, which in turn defines the final metal arrangement.

2. The model

A model was developed to simulate the kinetic course of the two chemical reductions (see Ref. [38] for details). The reaction medium is a microemulsion, which is described as a set of micelles. The one-pot method is reproduced by mixing equal volumes of three microemulsions, each of which contains one of the three reactants (two metal precursors and the reducing agent R). This pattern of mixing reactants recreates the one-pot method, by which the two metal salts are simultaneously reduced.

2.1 Initial reactants concentration

Reactants are initially distributed throughout micelles using a Poisson distribution, that is, the occupation of all micelles is not similar. In this study, we present results using different values of metal precursors concentration, but keeping a proportion 1:1 of the two metals: $\langle cAuCl_4^- \rangle = \langle cPtCl_6^{2-} \rangle = \langle c \rangle$ = 2, 16, 32, and 64 metal precursors in each micelle, which corresponds to 0.01, 0.08, 0.16, and 0.40 M, respectively, in a micelle with a radius of 4 nm. Au and Rh precursors ($AuCl_4^-$ and $RhCl_6^{3-}$) are represented by M^+. Calculations have been made under isolation conditions, that is, reducing agent R is in excess: ($\langle cR \rangle = 10\langle cPtCl_6^{2-} \rangle$).

2.2 Microemulsion dynamics and time unit

Micelles move and collide with each other. The intermicellar collision is a key feature in kinetics in microemulsions, because upon collision micelles are able to establish a water channel, which allows the exchange of their contents (metal precursors, reducing agent, metallic atoms, and/or growing particles). The material intermicellar exchange makes possible the reactant encounter inside micelles and, as a consequence, it is determinant of chemical reactions to occur. The intermicellar collision is simulated by choosing a 10% of micelles at random. These selected micelles collide, fuse (allowing material intermicellar exchange), and then redisperse. One Monte Carlo step begins in each intermicellar collision and ends when the quantity of species carried by colliding micelles is revised in agreement to the exchange criteria described below.

2.3 Metal characterization: reduction rate ratio

The reduction rate of a metal A (v_A) can be related to the standard potential (ε^0_A) by means of the Volmer equation:

$$\frac{j_A}{j_B} = \frac{v_A n_A F}{v_B n_B F} = \frac{n_A F k_{red,A} c_{O,A} \exp\left[-\frac{\beta_A n_A F \varepsilon_A}{RT}\right]}{n_B F k_{red,B} c_{O,B} \exp\left[-\frac{\beta_B n_B F \varepsilon_B}{RT}\right]} = \exp\left[\frac{\beta nF(\varepsilon_B - \varepsilon_A)}{RT}\right] \quad (1)$$

where j_A is the current density, n_A is the number of electrons, F is the Faraday constant, $k_{red,A}$ is the chemical rate constant, β_A is the transfer coefficient, $c_{O,A}$ is the concentration of oxidized A, R is the gas constant, and T is temperature. When two metals A and B, initially at the same concentration ($c_{O,A} = c_{O,B}$), are reduced simultaneously to synthesize an A/B bimetallic nanoparticle, this equation can be simplified by assuming the following approximations: the number of electrons ($n_A = n_B = n$), the transfer coefficients ($\beta_A = \beta_A = \beta$), and the chemical rate constants ($k_{red,A} = k_{red,B} = k_{red}$) are equal. (One must keep in mind that main factor governing reduction rates is by electrochemical potential.) Under this condition, a simple relation between the rates of electron transfer of two species A and B and their standard potentials can be deduced.

$$\log \frac{v_A}{v_B} = \frac{1}{2.3} \frac{\beta nF(\varepsilon_B - \varepsilon_A)}{RT} \quad (2)$$

This equation supports the rule according to which the higher the difference between the standard potentials of the two metals, the higher the ratio between both reduction rates is.

2.3.1 Au/Pt nanoparticles

On the basis of Eq. (2), to simulate the reduction rate of Au/Pt nanoparticles, the standard reduction potential must be taken into account. When the Au precursor is $AuCl_4^-$, the standard reduction potential is $\varepsilon^0(AuCl_4^-) = 0.926$ V, which is higher than that of Pt precursor $\varepsilon^0(PtCl_6^{2-} = 0.742$ V). This results in a faster formation rate of Au particles. In fact, Au is reduced so quickly that kinetics cannot be studied by conventional methods, so stopped flow techniques were needed [39]. The color change occurs instantaneously, so Au reduction was simulated as fast as possible, that is, 100% of Au precursors located in colliding micelles react to produce Au atoms, whenever the amount of reducing agent was enough. The reduction rate parameter of a metal A (v_A) is the percentage of reactants inside colliding micelles which are reduced during a collision to give rise to products (A atoms). Regarding to Pt, its reduction rate was successfully simulated by using $v_{Pt} = 10\%$, that is, only a 10% of Pt precursor reacts in each collision ($v_{Pt} = 10\%$) [40]. In this way, Au/Pt nanoparticle formation is simulated by a reduction rate ratio $v_{Au}/v_{Pt} = 100/10 = 10$, that is, Au reduction is 10 times faster than Pt.

The two reductions can take place simultaneously within the same micelle. The metal precursors and/or reducing agent that did not react remain behind in the micelle and will be exchanged or react later.

2.3.2 Pt/Rh nanoparticles

In order to research the influence of another metal in the pair Pt/M on Pt reduction, a metal whose reduction rate would be 10 times slower than Pt was chosen. In this manner, the reduction rate ratio is the same as used to simulate Au/Pt nanoparticles, so the possible differences in the kinetic behavior and the final metal distributions cannot be supported by the difference between the standard potentials. Therefore, the reduction rate of Pt is the same as that of Au/Pt pair ($v_{Pt} = 10\%$), but now Pt is the faster metal. Taking into account the standard reduction potential of $RhCl_6^{3-}$, $\varepsilon^0(RhCl_6^{3-}) = 0.44$ V, this Rh precursor is a good candidate to be simulated as $v_{Rh} = 1\%$ (only a 1% of $RhCl_6^{3-}$ located in the colliding micelles will be reduced ($v_{Pt}/v_{Rh} = 10/1 = 10$)).

The number of each species located within each micelle is adjusted at each step in agreement with the possibility of chemical reduction and the intermicellar

exchange criteria (see below). As the metallic atoms are produced in each micelle, they are assumed to be deposited on nanoparticle seed. That is, unlike for reactants, which are isolated within the micelle, all metal atoms inside a micelle are aggregated forming a growing nanoparticle. In order to calculate the metal distribution in the final bimetallic nanoparticle, the sequence of metals which are reduced is monitored in each micelle as a function of time.

2.4 Microemulsion characterization: intermicellar exchange criteria

Two different intermicellar exchange criteria are implemented depending on the nature of exchanged species. Metal precursor, reducing agent, and free metal atoms are isolated species, which will be redistributed between two colliding micelles in accordance with the concentration gradient principle: they are transferred from the more to the less occupied micelle. The exchange parameter k_{ex} quantifies the maximum amount of isolated species that can be exchanged during an intermicellar collision. As a result of this redistribution, the metal salts ($PtCl_6^{2-}$ and/or M^+) and the reducing agent R can be located within the same micelle. At this stage, chemical reduction can occur at a rate which depends on the nature of the metal.

As the reductions take place, metal atoms are produced within micelles. It is assumed that metal atoms are deposited on nanoparticle seed, so all metal atoms inside a micelle are considered to be aggregated forming a growing nanoparticle. The larger size of a growing nanoparticle leads to a second interdroplet exchange protocol. It is assumed that the exchange of growing particles is restricted by the size of the channel connecting colliding micelles. The ease with which this channel can be established as well as the channel size is mainly determined by the flexibility of the surfactant film. The flexibility parameter (f) specifies the maximum particle size for transfer between micelles. The exchange criterium of growing particles also takes into account Ostwald ripening, which assumes that larger particles grow by condensation of material, coming from the smaller ones that solubilize more readily than larger ones. This feature is included in the model by considering that if both colliding micelles carry a growing particle, the smaller one is exchanged towards the micelle carrying the larger one, whenever the channel size would be large enough.

As the synthesis advances, micelles can contain simultaneously reactants and growing particles. In this situation, autocatalysis can take place. Thus, if one of the colliding micelles is carrying a growing particle, the reaction always proceeds on it. If both colliding micelles contain particles, reaction takes place in the micelle containing the larger one, because it has a larger surface, so a higher probability of playing as catalyst.

Based on these simple criteria for material interdroplet exchange, surfactant film flexibility can be characterized as follows. There are two main requirements for material intermicellar exchange to occur: the size of the channel connecting colliding micelles must be large enough and the dimer formed by colliding micelles must be stable, that is, they must remain together long enough. Isolated species (reactants and free metals) traverse the intermicellar channel one by one, so one can assume that the key factor determining their exchange is the dimer stability. That is, when the two micelles stay together longer (higher dimer stability), a larger quantity of species can be exchanged. Channel size would not be relevant in this case. Based on this, k_{ex}, which quantifies how many units of isolated species can be exchanged during a collision, is related to the dimer stability. Conversely, when the transferred material is a particle constituted by aggregation of metal atoms, which travels through the channel as a whole, channel size becomes decisive. This kind of material exchange will be restricted by the intermicellar channel size (f parameter). From this picture, the flexibility of the surfactant film is simulated by means of these two parameters, k_{ex} (dimer stability) and f (intermicellar channel size).

A rigid film, such as AOT/n-heptane/water microemulsion, was successfully reproduced considering a channel size f = 5, associated to k_{ex} = 1 free atoms exchanged during a collision [26]. In case of flexible film, both factors rise together, because a more flexible film produces more stable dimer and larger channel size, allowing a quicker exchange of isolated species as well as an exchange of larger particles [41]. That is, a flexible film is associated to a faster material intermicellar exchange rate. A more flexible microemulsion, such as 75% Isooctane/20% Tergitol/5% water microemulsion, was successful compared to simulation data using the values f = 30, k_{ex} = 5 [42].

2.5 Description of the metal distribution in the bimetallic nanoparticle

The composition of each nanoparticle is revised at each step and monitored as a function of time. When all metal precursors were reduced and the content of all micelles remains constant over time, nanoparticle synthesis is considered to be finished. At this stage, the sequence of metal deposition of each particle (which is stored as a function of time) is stabilized. One simulation run produces a set of micelles, each one of them can carry one particle with different composition or be empty. At the end of each run, the averaged nanoparticle is calculated. Finally, results are averaged over 1000 runs.

The intrastructure of each particle is calculated by analyzing the sequence in which the two metals are deposited on the nanoparticle surface. So that, each sequence is arranged in 10 concentric layers, assuming that final nanoparticle is spherical. Then, the averaged percentage of each metal is calculated layer by layer. The final bimetallic distribution is represented by histograms, in which the layer composition is described by a color grading, as stated in the following pattern: Au, Pt, and Rh are represented by red, blue, and green, respectively. As the proportion of pure metal in the layer is higher, the color becomes lighter. In order to illustrate the heterogeneity of nanoparticle composition, the number of particles with a given percentage of the faster reduction metal (Au in Au/Pt and Pt in Pt/Rh nanoparticles) in each of 10 layers is also represented in the histograms. This analysis is reproduced layer by layer, from the beginning of the synthesis (inner layer or core) to the end (outer layer or surface). To simplify, the metal distribution is also shown by means of concentric spheres, whose thickness is proportional to the number of layers with the same composition, keeping the same color pattern.

3. Results and discussion

3.1 Factors affecting metal distribution: initial reactants concentration

The simulation model was successfully validated by comparison with experimental results. Au/Pt nanoparticles were synthesized in a 75% Isooctane/20% Tergitol/5% water microemulsion [42] (which can be characterized as flexible microemulsion)using different precursor concentrations. ($\langle cAuCl_4^- \rangle = \langle cPtCl_6^{2-} \rangle = \langle c \rangle$ = 0.01, 0.08, 0.16, and 0.40 M. The resulting Au/Pt particles were studied by HR-STEM and their structures were revealed by cross sections scanned with EDX analysis. The studied conditions were reproduced by simulation, using concentrations $\langle cAuCl_4^- \rangle = \langle cPtCl_6^{2-} \rangle = \langle c \rangle$ = 2, 16, 32, and 64 metal precursors in each micelle, which corresponds to 0.01, 0.08, 0.16, and 0.40 M, respectively, in a micelle with a radius of 4 nm. As mentioned above, Au/Pt pair was characterized as v_{Au}/v_{Pt} = 10 reduction rate ratio, and the 75% Isooctane/20% Tergitol/5% water microemulsion was simulated as a flexible surfactant film (f = 30, k_{ex} = 5).

The left column in **Figure 1** shows the simulated nanostructures obtained at each concentration. In order to compare the experimental and simulated nanostructures, the quantity of each metal crossed by a beam of 2 Å (approximate EDX beam size) was computed from each simulated final nanoparticle, and the theoretical STEM profiles were calculated. The STEM profiles of the average particle for each concentration are shown in center (theoretical) and right (experimental) columns of **Figure 1**. For a better comparison, experimental x-axis was changed from nm to counts, and the two kind of profiles were normalized to 1. Both profiles show the expected behavior: the surface (outer layers) is enriched in Pt, because of its slower reduction rate, and Au, which is reduced faster, accumulates in the core (inner layers). As concentration increases (see **Figure 1** from the top to the bottom), deeper Pt profiles are obtained. This means that the final nanostructure shows an improved metal segregation as concentration is higher. It is clearly observed in the histograms, which evolve from Au core covered by a mixed shell obtained at a low concentration to a more mixed Au core covered by a pure Pt shell as concentration

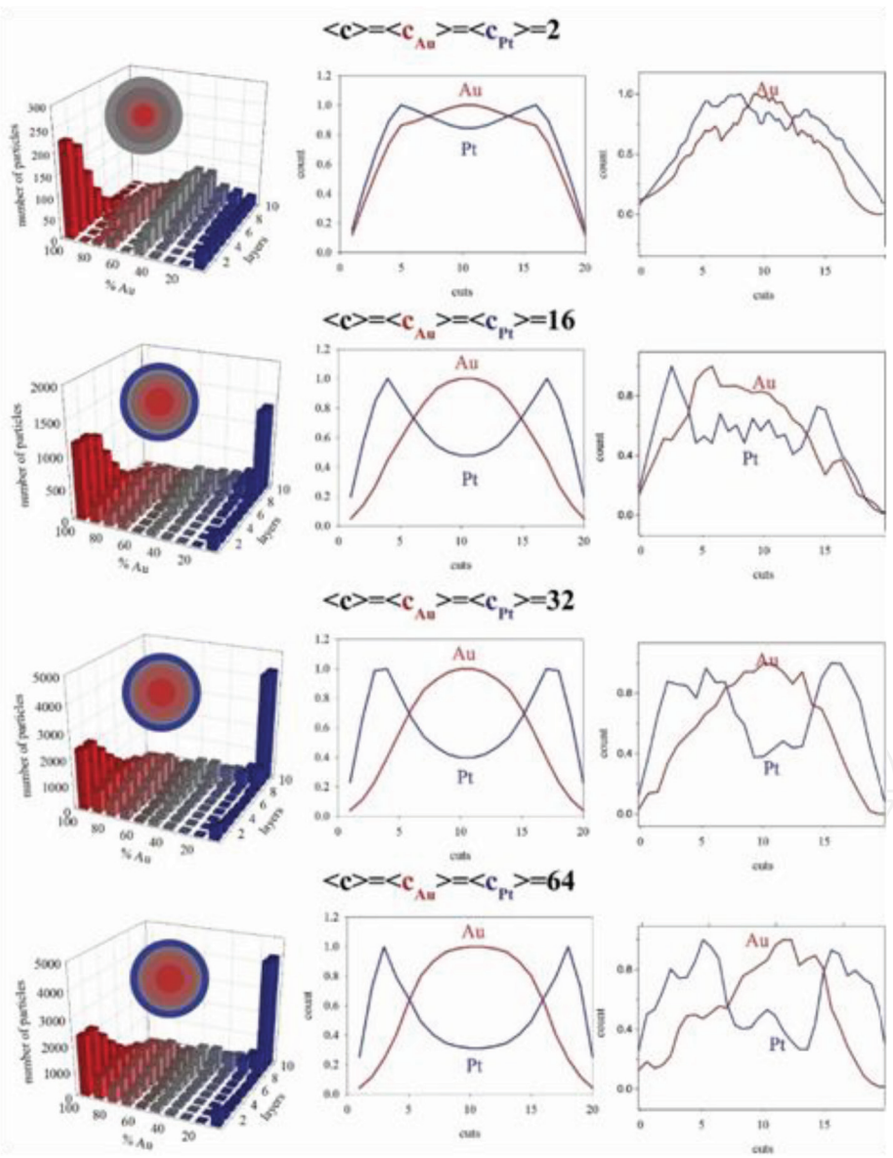

Figure 1.
Left column: simulated histograms for different initial concentrations (Au:Pt = 1:1). The proportion of pure metal in the layer is higher as the color becomes lighter (red: 100% Au, blue: 100% Pt, gray: 50% Au-Pt). Centre column: calculated STEM profiles for the average nanoparticle. Right column: measured STEM profiles for Au/Pt nanoparticles synthesized in a water/tergitol/isooctane microemulsion. Simulation parameters: flexible film (k_{ex} = 5, f = 30); reduction rate ratio (v_{Au}/v_{Pt} = 100/10); and reducing agent concentration $\langle cR \rangle = 10\langle M^{+} \rangle$. Adapted with permission from Ref. [42]. Copyright (2015) American Chemical Society.

increases (see decreasing red bar on the left and increasing blue bar on the right in histograms of **Figure 1**). This means that the nanostructure can be fine-tuned with sub-nanometer resolution, just by changing concentration.

A good agreement between experimental and theoretical results was attained, upholding the validity of the simulation model to predict the atomic structure of bimetallic nanoparticles. On this basis, the model becomes a strong tool to further enhance our knowledge of the complex mechanisms governing reactions in microemulsions and the impact of compartmentalization on final nanostructures.

The better metal segregation obtained as concentration increases is also observed when the two reductions are slowing down, as shown in **Figure 2**. This figure shows the final nanostructures obtained for the pair Pt/Rh (v_{Pt}/v_{Rh} = 10/1 = 10), under the same synthetic conditions as used in **Figure 1** to prepare Au/Pt nanoparticles. The better metal separation cannot be attributed to a larger reduction rate ratio, because in both cases the faster metal is 10 times faster than the slower one (v_{Au}/v_{Pt} = 100/10 = 10). The better metal separation obtained for Pt/Rh pair is more evident at low concentration, where an alloy is obtained for Au/Pt and a core-shell structure for Pt/Rh (compare histograms when $\langle c \rangle$ = 2 in **Figures 1** and **2**). This means that, although the reduction rate ratio is similar, when the reduction rate of the faster metal slows down as in Pt, the other metal (Rh) is delayed even more. As a consequence, both reactions take place at different stages of the synthesis, resulting in better segregated structures.

3.2 Factors affecting metal distribution: reduction rate ratio

The difference between the standard potentials of the two metal precursors is believed to be the most relevant factor to determine the kinetics and the resulting bimetallic arrangement [43]. As established in Eq. (2), the higher the difference between the standard potentials of the two metals, the higher the ratio between both reduction rates is. It results in the earlier reduction of the faster reduction metal, which builds up the core and becomes the seed for the subsequent deposition of the slower metal, which forms the surrounding shell. On the contrary, when the two reduction rates are almost similar, a mixed nanoalloy is expected. In spite of this argumentation was initially proposed for reactions in homogeneous media, and it does not take into account the confinement of reactants within micelles, it is frequently applied to explain results in microemulsion. As a rule, it is observed a tendency from nanoalloy to core-shell structure as difference in reduction potential is increased (see Table 1 in Ref. [44]). Previous simulation studies allow to clearly observe a better separation of the two metals as reduction rate ratio is larger (for a deeper discussion, see Ref. [28]).

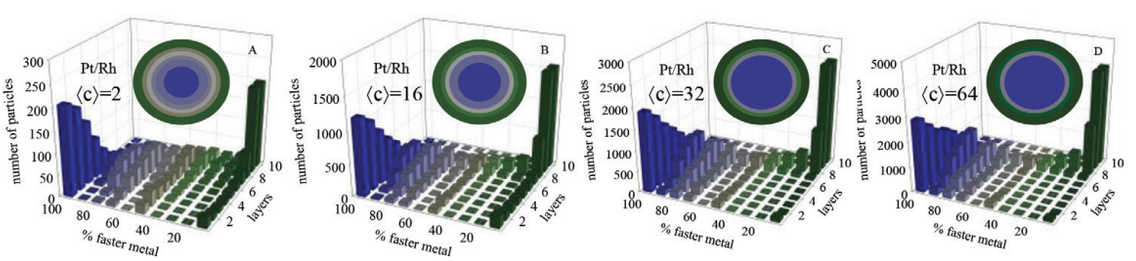

Figure 2.
Histograms show the number of particles with a given percentage of the faster reduction metal (Pt) in each layer at different concentrations. In all cases, $\langle cR \rangle = 10\langle cPtCl_6^{2-} \rangle$, and $cPtCl_6^{2-}$:$RhCl_6^{3-}$ is in 1:1 proportion. Reduction rates: v_{Pt} = 10%, v_{Rh} = 1% (v_{Pt}/v_{Rh} = 10); flexible film (f = 30, k_{ex} = 5). Scheme color: Pt and Rh are represented by blue and green bars, respectively. Lighter colors mean less mixture. The nanostructure is also shown by colored concentric spheres, keeping the same color pattern.

3.3 Factors affecting metal distribution: microemulsion composition

To isolate the effect of microemulsion composition on nanoparticle structure, a particular pair of metals must be chosen and analyze if a change in the microemulsion composition leads to a different metal segregation. For example, Pt/Ru nanoparticles were obtained as nanoalloy, both for rigid (water/Brij-30/n-heptane [45]) and flexible films (water/Berol 050/isooctane 80 [46] or water/NP5-NP9/cyclohexane [47]). But in this couple, the small difference in reduction potentials leads to quite similar reduction rates, which hinder metal segregation, even with a slow intermicellar exchange rate. As a matter of fact, when couples with higher reduction rate ratio are studied (such as Au/Ag, Au/Pt, and Au/Pd), an increase in surfactant flexibility results in the expected transition from a core-shell to a nanoalloy. As an example, alloyed Au/Pt nanoparticles were prepared using a flexible film such as water/Tergitol 15-S-5/isooctane [17] or water/TritonX-100/cyclohexane [48]. On the contrary, rigid films (water/AOT/isooctane [39] and water/Brij 30/n-heptane [49]) lead to segregated structures. The simulation model also predicts this result, as shown in **Figure 3**, in which different Au/Pt (v_{Au}/v_{Pt} = 10) arrangements were obtained by employing different values of surfactant film flexibilities. The ability of the microemulsion to minimize the difference between the reduction rates is clearly reflected in the progressive mixture of Au and Pt as increasing the intermicellar exchange rate (for a deeper discussion, see the following sections).

3.4 Kinetic study

The results shown in previous figures were obtained under isolation conditions, that is, the reducing agent concentration is much higher than stoichiometry, so the change in R concentration during the course of the reaction is negligible. As a result, the metal reduction, which is a bimolecular reaction, appears to be first order, when the reaction media is homogeneous. In order to study how the confinement of reactants inside micelles would affect chemical kinetics, the depletion of the number of metal precursors M^+ ($M^+ = AuCl_4^-$, $PtCl_{6-}^{2-}$, $RhCl_6^{3-}$) was monitored as the synthesis advances. The logarithmic plot of M^+ concentration versus time is shown in **Figure 4** using different initial reactant concentrations. Left and right columns show results for Au/Pt and Pt/Rh couples, respectively. Au, Pt, and Rh are represented by dashed, solid, and dashed-dotted lines, respectively. **Figure 4A** and **B** was obtained by simulating a flexible film and **C** and **D** a rigid one. At first

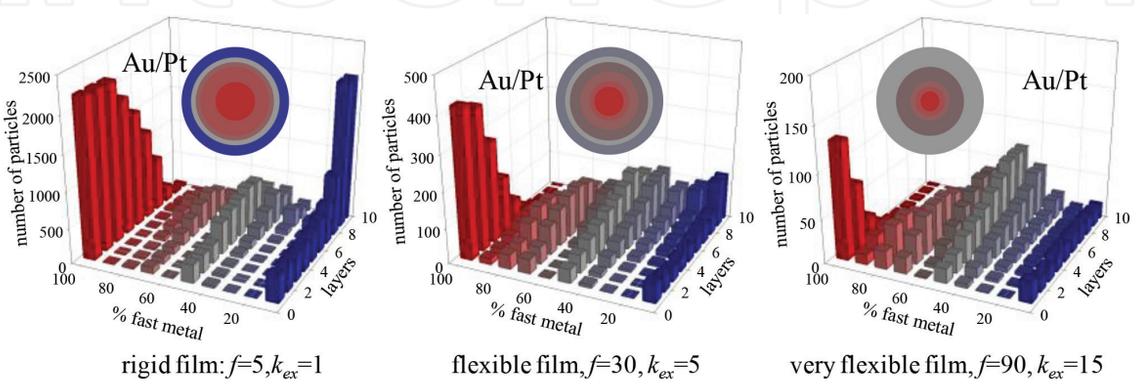

Figure 3.
Number of particles with a given percentage of the faster reduction metal (Au) in each layer using three different microemulsion compositions (different f and k_{ex} parameters). $\langle cAuCl_4^- \rangle = \langle cPtCl_6^{2-} \rangle = 4$; $\langle cR \rangle = 10\langle cPtCl_6^{2-} \rangle$ reduction rates: v_{Au} = 100%, v_{Pt} = 10%. Scheme color: Au and Pt are represented by red and blue bars, respectively. Lighter colors mean less mixture. Adapted with permission from Ref. [44].

sight, metal reductions obey first-order kinetics in both Au/Pt and Pt/Rh synthesis, as expected. Nevertheless, it is important to note that, with the exception of Rh, a time lag is required to reach the linear regime. Two points must be highlighted: First, the higher the concentration, the longer the time lag between the beginning of the synthesis and the achievement of the linear behavior. On the second hand, the time lag strongly depends on the intermicellar exchange rate, being longer as the exchange rate is slower (rigid film). Both factors (concentration and film flexibility) suggest that the rate-determining step is the intermicellar exchange rate at earlier reaction times, as explained as follows. The synthesis starts when the microemulsions containing the reactants are mixed. In order to be able to react, reactants must be located inside the same micelle. The reactants redistribution between micelles is dictated by the rate with which reactants can go through the channels communicating colliding micelles, that is, the intermicellar exchange rate. So, a slow exchange rate only allows the exchange of few reactants in each collision, which implies that more collisions are required to redistribute reactants and allow the reactants encounter. Therefore, a rigid film requires much longer lag times than a flexible one (compare **Figure 4A** with **B** and **C** with **D**, for any value of concentration). Apart from that, reactants redistribution is also affected by concentration, because the number of reactants which can traverse the intermicellar channel during an effective collision is restricted. Therefore, if concentration within micelle is large, more collisions (i.e., more time) are needed to make possible reactants redistribution. Finally, it is interesting to point out that this delay in reaching linear behavior disappears when a very slow chemical reduction takes place, as shown by Rh kinetics in right column of **Figure 4** (see dashed-dotted lines), which is linear from the beginning, at any

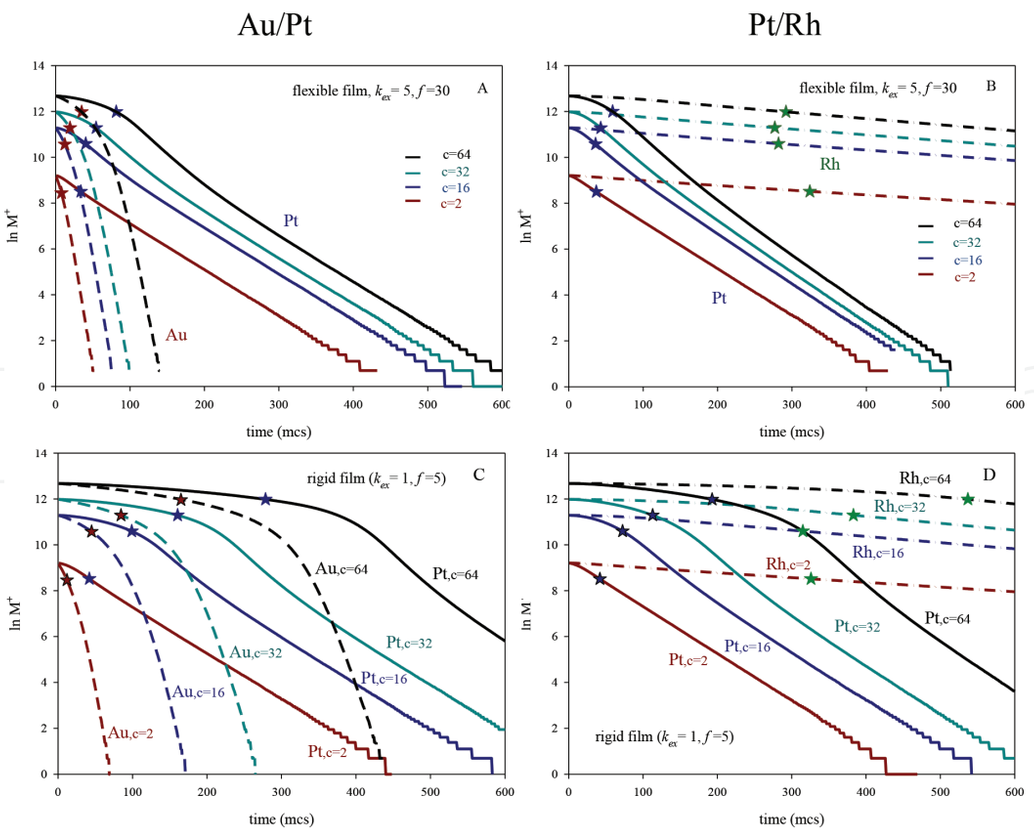

Figure 4.
Plot of ln M^+ (number of metal salt) against time (in Monte Carlo step, mcs) using different initial concentration c (metal salts/micelle). Solid, dashed, and dashed-dotted represent Au, Pt, and Rh, respectively. A and B shows results for a flexible surfactant film (k_{ex} = 5, f = 30) and C and D for a rigid one (k_{ex} = 1, f = 5). Au/Pt pair (v_{Au}/v_{Pt} = 100/10 = 10) is represented in A and C and Pt/Rh pair (v_{Pt}/v_{Rh} = 10/1 = 10) in B and D. Stars indicate the half-life (red, blue, and green means Au, Pt and Rh, respectively).

concentration value. This behavior can be taken as indication that the reduction rate is so slow (only a 1% of reactants give rise to products) that the limiting step is the reduction itself.

Summarizing, the time lag required to achieve linear behavior in **Figure 4** reflects the time it takes for reactants to encounter. This time lag can be determinant of final metal segregation, because the inner layers of nanoparticle are building up during this stage.

Pseudo-first-order rate constants, k_{obs}, can be calculated from linear regime of the logarithmic plot as shown in **Figure 4**. The values of the pseudo-first-order rate constants are represented in **Figure 5** as a function of concentration. One can observe that the slopes of Au reduction are always higher than the slopes of Pt, which in turn is faster that Rh, as expected. Classical chemical kinetics in a homogeneous reaction medium establishes that k_{obs} in bimolecular reactions does not depend on precursors concentrations. This is the case for Pt and Rh, whose k_{obs} values did not depend neither on the concentration nor on the intermicellar exchange rate. In contrast, k_{obs} values of Au are strongly influenced by both factors. To explain this behavior, one have to take into account that the limiting step in Au chemical reduction is the intermicellar exchange [38, 50], because of the extremely fast Au reduction rate. One can observe that the dependence of k_{obs} on concentration decreases as intermicellar exchange rate is faster, until reaching an almost constant value at very fast intermicellar exchange rate (see gray line in **Figure 5**), as expected. In comparison, Pt and Rh reductions are so slow that their rates are not limited by the exchange rate.

One can conclude from **Figure 5** that intermicellar exchange rate exerts a different degree of influence depending on the reduction rate of the metal in comparison to the intermicellar exchange rate. This means that the compartmentalization of reaction medium takes part in chemical kinetics more or less depending on the metal nature. This different interplay between exchange rate and reduction rate has to be reflected in the metal segregation of final nanoparticle. It was proposed that if the intermicellar exchange rate can only modify the rate of metals whose

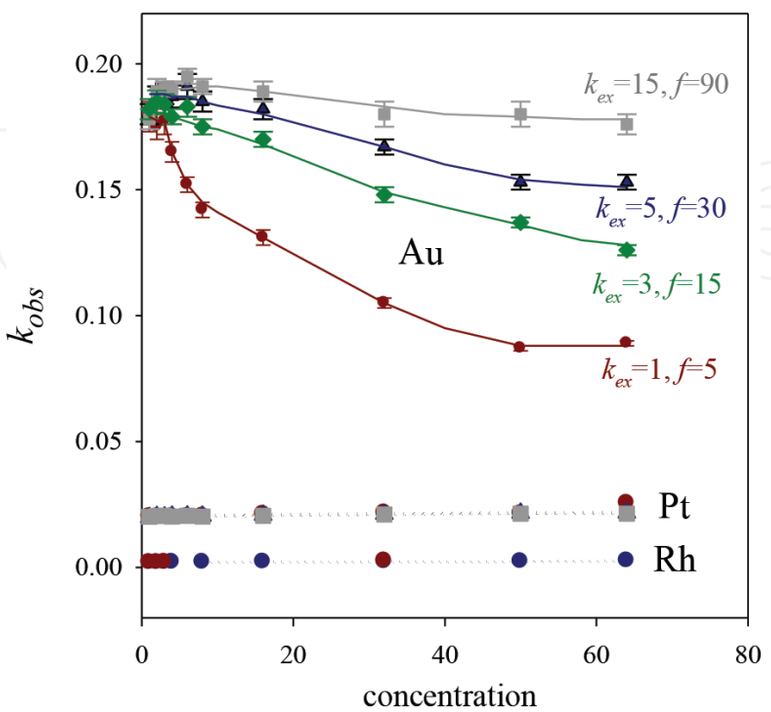

Figure 5.
k_{obs} (slopes of the linear parts from the plots in **Figure** *3) as a function of concentration for different microemulsion compositions and different metals. v_{Au} = 100, v_{Pt} = 10, v_{Rh} = 1. Lines are only a guide to the eye.*

reduction is very fast [38], such as Au, only bimetallic nanoparticle including Au could be prepared with different metal distributions as a function of microemulsion composition (intermicellar exchange rate) by a one-pot method (see Table 1 in Ref. [44]). To the best of our knowledge, only Au/Pt, Au/Ag, and Au/Pd have been synthesized in a different intrastructure by different authors. Thus, when a rigid film (such as provided by AOT) is used, Au-Pt nanoparticles are arranged in a core-shell distribution [39]. On the contrary, more flexible surfactants such as Brij30 [49], tergitol [17], or TritonX-100 [48] give rise to alloyed nanoparticles. In relation to Au/Ag, alloys were obtained with TritonX-100 [51] and $C_{11}E_3$ and $C_{11}E_5$ [52], but an enriched in Ag surface was observed when microemulsion contains AOT [53]. Finally, AOT was also used to obtain core-shell Au-Pd nanoparticles [54] and alloys with Pd-rich surface [55]. In contrast, true Au-Pd alloys [4] have been obtained with Brij30 and TritonX-100. With that in mind, it could be suggested that metal segregation in the nanoparticle can be modified by a change in the microemulsion composition only when one of the metals is Au or another very fast reduction rate metal. Nevertheless, in spite of the agreement between theoretical and experimental data, this assumption is based on the kinetic constants, which were calculated from the linear plot shown in **Figure 4**. It must be emphasized that the linear regime is not fulfilled at initial stages of the reaction, when the core is been building up. With the aim of studying the relevance of the non-linear behavior at the beginning of the synthesis, the half-life, defined as the time that it takes for the reactant concentration to decay to half of its initial value, was calculated for each case. Stars in **Figure 4** show half-life under different synthesis conditions (Au, Pt, and Rh are represented by red, blue, and green stars, respectively). With the exception of Rh and Pt at very low concentration, half-life is usually smaller than the time needed to achieve the linear regime. As observed in **Figure 4C** and **D**, Au and Pt reductions in a rigid microemulsion and at high concentration have a half-life much earlier than linear plot. This means that not only the initial layers but also the middle ones are formed under a nonlinear regime. So, chemical reductions are still not a first-order process during the formation of a large part of the particle (for a deeper discussion on life time, see Ref. [38]).

4. Conclusions

The generalized belief according to which the difference in the reduction potentials determines the intrastructure in a bimetallic nanoparticle should be improved. We propose that there are three potentially limiting factors which restrict chemical kinetics of bimetallic nanoparticles prepared from microemulsions: chemical reduction rate itself, exchange rate of reactants between micelles, and reactants concentration. The specific combination of these three factors determines the reaction rate of each metal, which in turn determines the sequence of metals deposition and the resulting bimetallic arrangement.

The kinetic study of Pt/M nanoparticles prepared via microemulsions under isolation conditions shows that chemical reductions are pseudo-first-order reactions, but not from the initial stages. At the beginning of the synthesis, the reactants encounter is dictated by the redistribution of reactants between micelles, which is controlled by the intermicellar exchange rate. As a result, the limiting step of faster reduction metals, such as Au, is the intermicellar exchange. On the contrary, microemulsion dynamics has a little effect if reduction rates are very slow (i.e., Rh). This means that compartmentalization of the reaction media has a different impact depending on the reduction rate of the particular metal. We are not referring only to the reduction rate of a metal in relation to the another metal

in the pair but also how fast the reduction takes place in relation to the intermicellar exchange rate. Specifically, for a given reduction rates ratio and keeping fixed microemulsion composition and concentration, the fact that the two reactions were slow (as in Pt/Rh) leads to a better metal segregation than if both reactions are faster (as in Au/Pt). Therefore, with the exception of very slow metal reduction as Rh, intermicellar exchange rate drastically impacts on chemical kinetics, particularly at the beginning of the synthesis. This is not a minor matter, because it will be reflected in the composition of the core and middle layers of the resulting nanoparticle. So, the ability of microemulsion to manipulate the sequence of metal deposition, when the metal reductions are quite fast in relation to the intermicellar exchange rate, can be used to design the experiments to synthesize bimetallic particles with ad hoc nanoarrangements. This ability disappears when the two chemical reductions are slow, because of chemically controlled kinetics.

In this paper, computer simulation has proved to be very useful tool to identify suitable synthesis parameters, which control metal segregation in a bimetallic nanoparticle. Further insights into the interplay between metal nature, exchange rate, and final bimetallic structure can be gained from kinetics studies.

Acknowledgements

This work was supported by MINECO, Spain (MAT2015-67458-P, co-financed with FERDER Funds), from the European Union's H2020 research and innovation programme under grant agreement No. 646155 (INSPIRED) and from Xunta de Galicia (Programa REDES ED431D-2017/18). D.B. thanks for the postdoc grant from Xunta de Galicia, Spain (POS-A/2013/018).

Conflict of interest

The authors declare no conflict of interest.

Notes/thanks/other declarations

This research is dedicated to Prof. Julio Casado Linarejos, who teached us the fundamentals of chemical kinetics.

Author details

Concha Tojo[1*], David Buceta[2] and M. Arturo López-Quintela[2]

1 Physical Chemistry Department, University of Vigo, Vigo, Spain

2 Laboratorio de Magnetismo y Nanotecnología, University of Santiago de Compostela, Santiago de Compostela, Spain

*Address all correspondence to: ctojo@uvigo.es

IntechOpen

References

[1] Boutonnet M, Kizling J, Stenius P, Maire G. The preparation of monodisperse colloidal metal particles from microemulsions. Colloids and Surfaces. 1982;**5**:209-225

[2] Sánchez-Dominguez M, Boutonnet M. Synthesis of nanostructured catalytic materials from microemulsions. Catalysts. 2016;**6**:4-8

[3] Heshmatpour F, Abazari R. Formation of dispersed palladium-nickel bimetallic nanoparticles in microemulsions: Synthesis, characterization, and their use as efficient heterogeneous recyclable catalysts for the amination reactions of aryl chlorides under mild conditions. RSC Advances. 2014;**4**:55815-55826

[4] Li T, Zhou H, Huang J, Yin J, Chen Z, et al. Facile preparation of Pd-Au bimetallic nanoparticles via in-situ self-assembly in reverse microemulsion and their electrocatalytic properties. Colloids and Surfaces, A: Physicochemical and Engineering Aspects. 2014;**463**:55-62

[5] Yuan P, Ma R, Gao N, Garai M, Xu Q-H. Plasmon coupling-enhanced two-photon photoluminescence of Au@Ag core-shell nanoparticles and applications in the nuclease assay. Nanoscale Research Letters. 2015;**7**:10233-10239

[6] Gao M-R, Xu Y-F, Jiang J, Yu S-H. Nanostructured metal chalcogenides: Synthesis, modification, and applications in energy conversion and storage devices. Chemical Society Reviews. 2013;**42**:2986-3017

[7] Tuaev X, Rudi S, Petkov V, Hoell A, Strasser P. In situ study of atomic structure transformations of Pt-Ni nanoparticle catalysts during electrochemical potential cycling. ACS Nano. 2013;**7**:5666-5674

[8] Gu X, Lu Z-H, Jiang H-L, Akita T, Xu Q. Synergistic catalysis of metal-organic framework-immobilized Au-Pd nanoparticles in dehydrogenation of formic acid for chemical hydrogen storage. Journal of the American Chemical Society. 2011;**133**:11822-11825

[9] Fletcher PDI, Howe AM, Robinson BH. The kinetics of solubilisate exchange between water droplets of a water-in-oil microemulsion. Journal of the Chemical Society, Faraday Transactions. 1987;**83**:985-1006

[10] Eriksson S, Nylen U, Rojas S, Boutonnet M. Preparation of catalysts from microemulsions and their applications in heterogeneous catalysis. Applied Catalysis A. 2004;**265**:207-219

[11] Boutonnet M, Lögdberg S, Svensson EE. Recent developments in the application of nanoparticles prepared from w/o microemulsions in heterogeneous catalysis. Current Opinion in Colloid & Interface Science. 2008;**13**:270-286

[12] Magno LMA, Angelescu DG, Sigle W, Stubenrauch C. Microemulsions as reaction media for the synthesis of Pt nanoparticles. Physical Chemistry Chemical Physics. 2011;**13**:3048-3058

[13] Eastoe J, Hollamby MJ, Hudson LK. Recent advances in nanoparticle synthesis with reversed micelles. Advances in Colloid and Interface Science. 2006;**128-130**:5-15

[14] Yashima M, Falk LKL, Palmqvist AEC, Holmberg K. Structure and catalytic properties of nanosized alumina supported platinum and palladium particles synthesized by reaction in microemulsion. Journal of Colloid and Interface Science. 2003;**268**:348-356

[15] Szumelda T, Drelinkiewicz A, Kosydar R, Góral-Kurbiel M, Gurgul J, Duraczynska D. Formation of Pd-group VIII bimetallic nanoparticles by the "water-in-oil" microemulsion method. Colloids and Surfaces, A: Physicochemical and Engineering Aspects. 2017;**529**:246-260

[16] Magno LM, Sigle W, van Aken PA, Angelescu D, Stubenrauch C. Size control of PtPb intermetallic nanoparticles prepared via microemulsions. Physical Chemistry Chemical Physics. 2011;**20**:9134-9136

[17] Hernández-Fernández P, Rojas S, Ocón P, Gómez de la Fuente JL, San Fabián J, et al. Influence of the preparation route of bimetallic Pt-Au nanoparticle electrocatalyst for the oxygen reduction reaction. The Journal of Physical Chemistry. B. 2007;**111**:2913-2923

[18] Summers M, Eastoe J, Davis S. Formation of $BaSO_4$ nanoparticles in microemulsions with polymerized surfactant shells. Langmuir. 2002;**18**:5023-5026

[19] Holmberg K. Surfactant-templated nanomaterials synthesis. Journal of Colloid and Interface Science. 2004;**274**:355-364

[20] Sánchez-Domínguez M, Aubery C, Solans C. New trends on the synthesis of inorganic nanoparticles using microemulsions as confined reaction media. In: Hashim A, editor. Smart Nanoparticles Technology. Rijeka: Intech; 2012

[21] Aubry J-M, Bouttemy S. Preparative oxidation of organic compounds in microemulsions with singlet oxygen generated chemically by the sodium molybdate/hydrogen peroxide system. Journal of the American Chemical Society. 1997;**119**:5286-5294

[22] Holmberg K. Organic reactions in microemulsions. European Journal of Organic Chemistry. 2007;**5**:723-728

[23] Parapat RY, Wijaya M, Schwarze M, Selve S, Willinger M, Schomäcker R. Particle shape optimization by changing from an isotropic to an anisotropic nanostructure: Preparation of highly active and stable supported Pt catalysts in microemulsions. Nanoscale Research Letters. 2013;**5**:796-805

[24] Parapat RY, Parwoto V, Schwarze M, Zhang B, Su D-S, Schomäcker R. A new method to synthesize very active and stable supported metal Pt catalysts: Thermo-destabilization of microemulsions. Journal of Materials Chemistry. 2012;**22**:11605-11614

[25] König RYG, Schwarze M, Schomäcker R, Stubenrauch C. Catalytic activity of mono- and bi-metallic nanoparticles synthesized via microemulsions. Catalysts. 2014;**4**:256-275

[26] Tojo C, Blanco MC, López-Quintela MA. Preparation of nanoparticles in microemulsions: A Monte Carlo study of the influence of the synthesis variables. Langmuir. 1997;**13**:4527-4534

[27] Magno LM, Sigle W, Aken PAV, Angelescu DG, Stubenrauch C. Microemulsions as reaction media for the synthesis of bimetallic nanoparticles: Size and composition of particles. Chemistry of Materials. 2010;**22**:6263-6271

[28] Tojo C, de Dios M, López-Quintela MA. On the structure of bimetallic nanoparticles synthesized in microemulsions. Journal of Physical Chemistry C. 2009;**113**:19145-19154

[29] Stamenkovic VR, Mun BS, Arenz M, Mayrhofer KJ, Lucas CA, et al. Trends in electrocatalysis on extended and nanoscale Pt-bimetallic alloy surfaces. Nature Materials. 2007;**6**:241-247

[30] Shi J. On the synergetic catalytic effect in heterogeneous nanocomposite catalysts. Chemical Reviews. 2013;**113**:2139-2181

[31] Ferrando R, Jellinek J, Johnston RL. Nanoalloys: From theory to applications of alloy clusters and nanoparticles. Chemical Reviews. 2008;**108**:845-910

[32] Spanos I, Dideriksen K, Kirkensgaard JJK, Jelavic S, Arenz M. Structural disordering of de-alloyed Pt bimetallic nanocatalysts: The effect on oxygen reduction reaction activity and stability. Physical Chemistry Chemical Physics. 2015;**17**:28044-28053

[33] Zhang G-R, Zhao D, Feng Y-Y, Zhang B, Su DS, et al. Catalytic Pt-on-au nanostructures: Why Pt becomes more active on smaller au particles. ACS Nano. 2012;**6**:2226-2236

[34] Shao M, Peles A, Shoemaker K, Gummalla M, Njoki PN, et al. Enhanced oxygen reduction activity of platinum monolayer on gold nanoparticles. Journal of Physical Chemistry Letters. 2011;**2**:67-72

[35] Notar Francesco I, Fontaine-Vive F, Antoniotti S. Synergy in the catalytic activity of bimetallic nanoparticles and new synthetic methods for the preparation of fine chemicals. ChemCatChem. 2014;**6**:2784-2791

[36] Zhao L, Thomas JP, Heinig NF, Abd-Ellah M, Wang X, Leung KT. Au-Pt alloy nanocatalysts for electro-oxidation of methanol and their application for fast-response non-enzymatic alcohol sensing. Journal of Materials Chemistry C. 2014;**2**:2707-2714

[37] Yin Z, Ma D, Bao X. Emulsion-assisted synthesis of monodisperse binary metal nanoparticles. Chemical Communications. 2010;**46**:1344-1346

[38] Tojo C, Buceta D, López-Quintela MA. Bimetallic nanoparticles synthesized in microemulsions: A computer simulation study on relationship between kinetics and metal segregation. Journal of Colloid and Interface Science. 2018;**510**:152-161

[39] Wu M, Chen D, Huang T. Preparation of Au/Pt bimetallic nanoparticles in water-in-oil microemulsions. Chemistry of Materials. 2001;**13**:599-606

[40] Tojo C, Buceta D, López-Quintela MA. Understanding the metal distribution in core-shell nanoparticles prepared in micellar media. Nanoscale Research Letters. 2015;**10**:339-349

[41] Quintillán S, Tojo C, Blanco MC, López-Quintela MA. Effects of the intermicellar exchange on the size control of nanoparticles synthesized in microemulsions. Langmuir. 2001;**17**:7251-7254

[42] Buceta D, Tojo C, Vukmirovik M, Deepak FL, López-Quintela MA. Controlling bimetallic nanostructures by the microemulsion method with sub-nanometer resolution using a prediction model. Langmuir. 2015;**31**:7435-7439

[43] Feng J, Zhang C. Preparation of Cu-Ni alloy nanocrystallites in water-in-oil microemulsions. Journal of Colloid and Interface Science. 2006;**293**:414-420

[44] Tojo C, Buceta D, López-Quintela MA. On metal segregation of bimetallic nanocatalysts prepared by a one-pot method in microemulsions. Catalysts. 2017;**7**:1-17

[45] Solla-Gullón J, Vidal-Iglesias FJ, Montiel V, Aldaz A. Electrochemical characterization of platinum-ruthenium nanoparticles prepared by water-in-oil microemulsion. Electrochimica Acta. 2004;**49**:5079-5088

[46] Rojas S, García-García FJ, Jaeras S, Martínez-Huerta MV, García Fierro JL, Boutonnet M. Preparation of carbon supported Pt and PtRu nanoparticles from microemulsion. Applied Catalysis, A: General. 2005;**285**:24-35

[47] Liu Z, Lee JY, Han M, Chen W, Gan LM. Synthesis and characterization of PtRu/C catalysts from microemulsions and emulsions. Journal of Materials Chemistry. 2002;**12**:2453-2458

[48] Pal A. Gold–platinum alloy nanoparticles through water-in-oil microemulsion. Journal of Nanostructure in Chemistry. 2015;**5**:65-69

[49] Habrioux A, Vogel W, Guinel M, Guetaz L, Servat K, et al. Structural and electrochemical studies of Au-Pt nanoalloys. Physical Chemistry Chemical Physics. 2009;**11**:3573-3579

[50] Tojo C, de Dios M, Buceta D, López-Quintela MA. Cage-like effect in Au-Pt nanoparticle synthesis in microemulsions: A simulation study. Physical Chemistry Chemical Physics. 2014;**16**:19720-19731

[51] Pal A, Shah S, Devi S. Preparation of silver, gold and silver-gold bimetallic nanoparticles in w/o microemulsion containing triton X-100. Colloids and Surfaces, A: Physicochemical and Engineering Aspects. 2007;**302**:483-487

[52] Cheng J, Bordes R, Olsson E, Holmberg K. One-pot synthesis of porous gold nanoparticles by preparation of Ag/Au nanoparticles followed by dealloying. Colloids and Surfaces, A: Physicochemical and Engineering Aspects. 2013;**436**:823-829

[53] Chen D, Chen C. Formation and characterization of Au-Ag bimetallic nanoparticles in water-in-oil microemulsions. Journal of Materials Chemistry. 2002;**12**:1557-1562

[54] Wu M, Chen D, Huang T. Synthesis of au/Pd bimetallic nanoparticles in reverse micelles. Langmuir. 2001;**17**:3877-3883

[55] Simoes M, Baranton S, Coutanceau C. Electrooxidation of sodium borohydride at Pd, au, and Pd_xAu_{1-x} carbon-supported nanocatalysts. Journal of Physical Chemistry C. 2009;**113**:13369-13376